

A search of the Orion spur for continuous gravitational waves using a "loosely coherent" algorithm on data from LIGO interferometers.

J. Aasi,¹ B. P. Abbott,¹ R. Abbott,¹ T. D. Abbott,² M. R. Abernathy,¹ F. Acernese,^{3,4} K. Ackley,⁵ C. Adams,⁶ T. Adams,^{7,8} P. Addesso,⁹ R. X. Adhikari,¹ V. B. Adya,¹⁰ C. Affeldt,¹⁰ M. Agathos,¹¹ K. Agatsuma,¹¹ N. Aggarwal,¹² O. D. Aguiar,¹³ A. Ain,¹⁴ P. Ajith,¹⁵ B. Allen,^{10,16,17} A. Allocca,^{18,19} D. V. Amariutei,⁵ M. Andersen,²⁰ S. B. Anderson,¹ W. G. Anderson,¹⁶ K. Arai,¹ M. C. Araya,¹ C. C. Arceneaux,²¹ J. S. Areeda,²² N. Arnaud,²³ G. Ashton,²⁴ S. M. Aston,⁶ P. Astone,²⁵ P. Aufmuth,¹⁷ C. Aulbert,¹⁰ S. Babak,²⁶ P. T. Baker,²⁷ F. Baldaccini,^{28,29} G. Ballardín,³⁰ S. W. Ballmer,³¹ J. C. Barayoga,¹ S. E. Barclay,³² B. C. Barish,¹ D. Barker,³³ F. Barone,^{3,4} B. Barr,³² L. Barsotti,¹² M. Barsuglia,³⁴ J. Bartlett,³³ M. A. Barton,³³ I. Bartos,³⁵ R. Bassiri,²⁰ A. Basti,^{36,19} J. C. Batch,³³ C. Baune,¹⁰ V. Bavigadda,³⁰ B. Behnke,²⁶ M. Bejger,³⁷ C. Belczynski,³⁸ A. S. Bell,³² B. K. Berger,¹ J. Bergman,³³ G. Bergmann,¹⁰ C. P. L. Berry,³⁹ D. Bersanetti,^{40,41} A. Bertolini,¹¹ J. Betzwieser,⁶ S. Bhagwat,³¹ R. Bhandare,⁴² I. A. Bilenko,⁴³ G. Billingsley,¹ J. Birch,⁶ R. Birney,⁴⁴ S. Biscans,¹² M. Bitossi,³⁰ C. Biwer,³¹ M. A. Bizouard,²³ J. K. Blackburn,¹ C. D. Blair,⁴⁵ D. Blair,⁴⁵ S. Bloemen,^{11,46} O. Bock,¹⁰ T. P. Bodiya,¹² M. Boer,⁴⁷ G. Bogaert,⁴⁷ P. Bojtos,⁴⁸ C. Bond,³⁹ F. Bondu,⁴⁹ R. Bonnand,⁸ R. Bork,¹ M. Born,¹⁰ V. Boschi,^{19,36} Sukanta Bose,^{14,50} C. Bradaschia,¹⁹ P. R. Brady,¹⁶ V. B. Braginsky,⁴³ M. Branchesi,^{51,52} V. Branco,⁵³ J. E. Brau,⁵⁴ T. Briant,⁵⁵ A. Brillet,⁴⁷ M. Brinkmann,¹⁰ V. Brisson,²³ P. Brockill,¹⁶ A. F. Brooks,¹ D. A. Brown,³¹ D. Brown,⁵ D. D. Brown,³⁹ N. M. Brown,¹² C. C. Buchanan,² A. Buikema,¹² T. Bulik,³⁸ H. J. Bulten,^{56,11} A. Buonanno,^{57,26} D. Buskulic,⁸ C. Buy,³⁴ R. L. Byer,²⁰ L. Cadonati,⁵⁸ G. Cagnoli,⁵⁹ J. Calderón Bustillo,⁶⁰ E. Calloni,^{61,4} J. B. Camp,⁶² K. C. Cannon,⁶³ J. Cao,⁶⁴ C. D. Capano,¹⁰ E. Capocasa,³⁴ F. Carbognani,³⁰ S. Caride,⁶⁵ J. Casanueva Diaz,²³ C. Casentini,^{66,67} S. Caudill,¹⁶ M. Cavaglià,²¹ F. Cavalier,²³ R. Cavalieri,³⁰ C. Celerier,²⁰ G. Cella,¹⁹ C. Cepeda,¹ L. Cerboni Baiardi,^{51,52} G. Cerretani,^{36,19} E. Cesarini,^{66,67} R. Chakraborty,¹ T. Chalermongsak,¹ S. J. Chamberlin,¹⁶ S. Chao,⁶⁸ P. Charlton,⁶⁹ E. Chassande-Mottin,³⁴ X. Chen,^{55,45} Y. Chen,⁷⁰ C. Cheng,⁶⁸ A. Chincarini,⁴¹ A. Chiummo,³⁰ H. S. Cho,⁷¹ M. Cho,⁵⁷ J. H. Chow,⁷² N. Christensen,⁷³ Q. Chu,⁴⁵ S. Chua,⁵⁵ S. Chung,⁴⁵ G. Ciani,⁵ F. Clara,³³ J. A. Clark,⁵⁸ F. Cleva,⁴⁷ E. Coccia,^{66,74} P.-F. Cohadon,⁵⁵ A. Colla,^{75,25} C. G. Collette,⁷⁶ M. Colombini,²⁹ M. Constanicio Jr.,¹³ A. Conte,^{75,25} L. Conti,⁷⁷ D. Cook,³³ T. R. Corbitt,² N. Cornish,²⁷ A. Corsi,⁷⁸ C. A. Costa,¹³ M. W. Coughlin,⁷³ S. B. Coughlin,⁷ J.-P. Coulon,⁴⁷ S. T. Countryman,³⁵ P. Couvares,³¹ D. M. Coward,⁴⁵ M. J. Cowart,⁶ D. C. Coyne,¹ R. Coyne,⁷⁸ K. Craig,³² J. D. E. Creighton,¹⁶ T. Creighton,⁸¹ J. Cripe,² S. G. Crowder,⁷⁹ A. Cumming,³² L. Cunningham,³² E. Cuoco,³⁰ T. Dal Canton,¹⁰ M. D. Damjanic,¹⁰ S. L. Danilishin,⁴⁵ S. D'Antonio,⁶⁷ K. Danzmann,^{17,10} N. S. Darman,⁸⁰ V. Dattilo,³⁰ I. Dave,⁴² H. P. Daveloza,⁸¹ M. Davies,²³ G. S. Davies,³² E. J. Daw,⁸² R. Day,³⁰ D. DeBra,²⁰ G. Debreczeni,⁸³ J. Degallaix,⁵⁹ M. De Laurentis,^{61,4} S. Deléglise,⁵⁵ W. Del Pozzo,³⁹ T. Denker,¹⁰ T. Dent,¹⁰ H. Dereli,⁴⁷ V. Dergachev,¹ R. De Rosa,^{61,4} R. T. DeRosa,² R. DeSalvo,⁹ S. Dhurandhar,¹⁴ M. C. Díaz,⁸¹ L. Di Fiore,⁴ M. Di Giovanni,^{75,25} A. Di Lieto,^{36,19} I. Di Palma,²⁶ A. Di Virgilio,¹⁹ G. Dojcinoski,⁸⁴ V. Dolique,⁵⁹ E. Dominguez,⁸⁵ F. Donovan,¹² K. L. Dooley,^{1,21} S. Doravari,⁶ R. Douglas,³² T. P. Downes,¹⁶ M. Drago,^{86,87} R. W. P. Drever,¹ J. C. Driggers,¹ Z. Du,⁶⁴ M. Ducrot,⁸ S. E. Dwyer,³³ T. B. Edo,⁸² M. C. Edwards,⁷³ M. Edwards,⁷ A. Effler,² H.-B. Eggenstein,¹⁰ P. Ehrens,¹ J. M. Eichholz,⁵ S. S. Eikenberry,⁵ R. C. Essick,¹² T. Etzel,¹ M. Evans,¹² T. M. Evans,⁶ R. Everett,⁸⁸ M. Factourovich,³⁵ V. Fafone,^{66,67,74} S. Fairhurst,⁷ Q. Fang,⁴⁵ S. Farinon,⁴¹ B. Farr,⁸⁹ W. M. Farr,³⁹ M. Favata,⁸⁴ M. Fays,⁷ H. Fehrmann,¹⁰ M. M. Fejer,²⁰ D. Feldbaum,^{5,6} I. Ferrante,^{36,19} E. C. Ferreira,¹³ F. Ferrini,³⁰ F. Fidecaro,^{36,19} I. Fiori,³⁰ R. P. Fisher,³¹ R. Flaminio,⁵⁹ J.-D. Fournier,⁴⁷ S. Franco,²³ S. Frasca,^{75,25} F. Frasconi,¹⁹ M. Frede,¹⁰ Z. Frei,⁴⁸ A. Freise,³⁹ R. Frey,⁵⁴ T. T. Fricke,¹⁰ P. Fritschel,¹² V. V. Frolov,⁶ P. Fulda,⁵ M. Fyffe,⁶ H. A. G. Gabbard,²¹ J. R. Gair,⁹⁰ L. Gammaitoni,^{28,29} S. G. Gaonkar,¹⁴ F. Garufi,^{61,4} A. Gatto,³⁴ N. Gehrels,⁶² G. Gemme,⁴¹ B. Gendre,⁴⁷ E. Genin,³⁰ A. Gennai,¹⁹ L. Á. Gergely,⁹¹ V. Germain,⁸ A. Ghosh,¹⁵ S. Ghosh,^{11,46} J. A. Giaime,^{2,6} K. D. Giardina,⁶ A. Giazotto,¹⁹ J. R. Gleason,⁵ E. Goetz,^{10,65} R. Goetz,⁵ L. Gondan,⁴⁸ G. González,² J. Gonzalez,^{36,19} A. Gopakumar,⁹² N. A. Gordon,³² M. L. Gorodetsky,⁴³ S. E. Gossan,⁷⁰ M. Gosselin,³⁰ S. Goßler,¹⁰ R. Gouaty,⁸ C. Graef,³² P. B. Graff,^{62,57} M. Granata,⁵⁹ A. Grant,³² S. Gras,¹² C. Gray,³³ G. Greco,^{51,52} P. Groot,⁴⁶ H. Grote,¹⁰ K. Grover,³⁹ S. Grunewald,²⁶ G. M. Guidi,^{51,52} C. J. Guido,⁶ X. Guo,⁶⁴ A. Gupta,¹⁴ M. K. Gupta,⁹³ K. E. Gushwa,¹ E. K. Gustafson,¹ R. Gustafson,⁶⁵ J. J. Hacker,²² B. R. Hall,⁵⁰ E. D. Hall,¹ D. Hammer,¹⁶ G. Hammond,³² M. Haney,⁹² M. M. Hanke,¹⁰ J. Hanks,³³ C. Hanna,⁸⁸ M. D. Hannam,⁷ J. Hanson,⁶ T. Hardwick,² J. Harms,^{51,52} G. M. Harry,⁹⁴ I. W. Harry,²⁶ M. J. Hart,³² M. T. Hartman,⁵ C.-J. Haster,³⁹ K. Haughian,³² A. Heidmann,⁵⁵ M. C. Heintze,^{5,6} H. Heitmann,⁴⁷ P. Hello,²³ G. Hemming,³⁰ M. Hendry,³² I. S. Heng,³² J. Hennig,³² A. W. Heptonstall,¹ M. Heurs,¹⁰ S. Hild,³² D. Hoak,⁹⁵ K. A. Hodge,¹ J. Hoelscher-Obermaier,¹⁷

- D. Hofman,⁵⁹ S. E. Hollitt,⁹⁶ K. Holt,⁶ P. Hopkins,⁷ D. J. Hosken,⁹⁶ J. Hough,³² E. A. Houston,³² E. J. Howell,⁴⁵
Y. M. Hu,³² S. Huang,⁶⁸ E. A. Huerta,⁹⁷ D. Huet,²³ B. Hughey,⁵³ S. Husa,⁶⁰ S. H. Huttner,³² M. Huynh,¹⁶
T. Huynh-Dinh,⁶ A. Idrisy,⁸⁸ N. Indik,¹⁰ D. R. Ingram,³³ R. Inta,⁷⁸ G. Islas,²² J. C. Isler,³¹ T. Isogai,¹²
B. R. Iyer,¹⁵ K. Izumi,³³ M. B. Jacobson,¹ H. Jang,⁹⁸ P. Jaranowski,⁹⁹ S. Jawahar,¹⁰⁰ Y. Ji,⁶⁴ F. Jiménez-Forteza,⁶⁰
W. W. Johnson,² D. I. Jones,²⁴ R. Jones,³² R.J.G. Jonker,¹¹ L. Ju,⁴⁵ Haris K,¹⁰¹ V. Kalogera,¹⁰² S. Kandhasamy,²¹
G. Kang,⁹⁸ J. B. Kanner,¹ S. Karki,⁵⁴ J. L. Karlen,⁹⁵ M. Kasprzak,^{23,30} E. Katsavounidis,¹² W. Katzman,⁶
S. Kaufer,¹⁷ T. Kaur,⁴⁵ K. Kawabe,³³ F. Kawazoe,¹⁰ F. Kéfélian,⁴⁷ M. S. Kehl,⁶³ D. Keitel,¹⁰ N. Kelecsenyi,⁴⁸
D. B. Kelley,³¹ W. Kells,¹ J. Kerrigan,⁹⁵ J. S. Key,⁸¹ F. Y. Khalili,⁴³ Z. Khan,⁹³ E. A. Khazanov,¹⁰³
N. Kijbunchoo,³³ C. Kim,⁹⁸ K. Kim,¹⁰⁴ N. G. Kim,⁹⁸ N. Kim,²⁰ Y.-M. Kim,⁷¹ E. J. King,⁹⁶ P. J. King,³³
D. L. Kinzel,⁶ J. S. Kissel,³³ S. Klimenko,⁵ J. T. Kline,¹⁶ S. M. Koehlenbeck,¹⁰ K. Kokeyama,² S. Koley,¹¹
V. Kondrashov,¹ M. Korobko,¹⁰ W. Z. Korth,¹ I. Kowalska,³⁸ D. B. Kozak,¹ V. Kringel,¹⁰ B. Krishnan,¹⁰
A. Królak,^{105,106} C. Krueger,¹⁷ G. Kuehn,¹⁰ A. Kumar,⁹³ P. Kumar,⁶³ L. Kuo,⁶⁸ A. Kutynia,¹⁰⁵ B. D. Lackey,³¹
M. Landry,³³ B. Lantz,²⁰ P. D. Lasky,^{80,107} A. Lazzarini,¹ C. Lazzaro,^{58,77} P. Leaci,^{26,75} S. Leavey,³²
E. O. Lebigot,^{34,64} C. H. Lee,⁷¹ H. K. Lee,¹⁰⁴ H. M. Lee,¹⁰⁸ J. Lee,¹⁰⁴ J. P. Lee,¹² M. Leonardi,^{86,87} J. R. Leong,¹⁰
N. Leroy,²³ N. Letendre,⁸ Y. Levin,¹⁰⁷ B. M. Levine,³³ J. B. Lewis,¹ T. G. F. Li,¹ A. Libson,¹² A. C. Lin,²⁰
T. B. Littenberg,¹⁰² N. A. Lockerbie,¹⁰⁰ V. Lockett,²² D. Lodhia,³⁹ J. Logue,³² A. L. Lombardi,⁹⁵ M. Lorenzini,⁷⁴
V. Lorette,¹⁰⁹ M. Lormand,⁶ G. Losurdo,⁵² J. D. Lough,^{31,10} M. J. Lubinski(Ski),³³ H. Lück,^{17,10} A. P. Lundgren,¹⁰
J. Luo,⁷³ R. Lynch,¹² Y. Ma,⁴⁵ J. Macarthur,³² E. P. Macdonald,⁷ T. MacDonald,²⁰ B. Machenschalk,¹⁰
M. MacInnis,¹² D. M. Macleod,² D. X. Madden-Fong,²⁰ F. Magaña-Sandoval,³¹ R. M. Magee,⁵⁰ M. Mageswaran,¹
E. Majorana,²⁵ I. Maksimovic,¹⁰⁹ V. Malvezzi,^{66,67} N. Man,⁴⁷ I. Mandel,³⁹ V. Mandic,⁷⁹ V. Mangano,^{75,25,32}
N. M. Mangini,⁹⁵ G. L. Mansell,⁷² M. Manske,¹⁶ M. Mantovani,³⁰ F. Marchesoni,^{110,29} F. Marion,⁸ S. Márka,³⁵
Z. Márka,³⁵ A. S. Markosyan,²⁰ E. Maros,¹ F. Martelli,^{51,52} L. Martellini,⁴⁷ I. W. Martin,³² R. M. Martin,⁵
D. V. Martynov,¹ J. N. Marx,¹ K. Mason,¹² A. Masserot,⁸ T. J. Massinger,³¹ F. Matichard,¹² L. Matone,³⁵
N. Mavalvala,¹² N. Mazumder,⁵⁰ G. Mazzolo,¹⁰ R. McCarthy,³³ D. E. McClelland,⁷² S. McCormick,⁶
S. C. McGuire,¹¹¹ G. McIntyre,¹ J. McIver,⁹⁵ S. T. McWilliams,⁹⁷ D. Meacher,⁴⁷ G. D. Meadors,¹⁰ M. Mehmet,¹⁰
J. Meidam,¹¹ M. Meinders,¹⁰ A. Melatos,⁸⁰ G. Mendell,³³ R. A. Mercer,¹⁶ M. Merzougui,⁴⁷ S. Meshkov,¹
C. Messenger,³² C. Messick,⁸⁸ P. M. Meyers,⁷⁹ F. Mezzani,^{25,75} H. Miao,³⁹ C. Michel,⁵⁹ H. Middleton,³⁹
E. E. Mikhailov,¹¹² L. Milano,^{61,4} J. Miller,¹² M. Millhouse,²⁷ Y. Minenkov,⁶⁷ J. Ming,²⁶ S. Mirshekari,¹¹³
C. Mishra,¹⁵ S. Mitra,¹⁴ V. P. Mitrofanov,⁴³ G. Mitselmakher,⁵ R. Mittleman,¹² B. Moe,¹⁶ A. Moggi,¹⁹
M. Mohan,³⁰ S. R. P. Mohapatra,¹² M. Montani,^{51,52} B. C. Moore,⁸⁴ D. Moraru,³³ G. Moreno,³³ S. R. Morris,⁸¹
K. Mossavi,¹⁰ B. Mours,⁸ C. M. Mow-Lowry,³⁹ C. L. Mueller,⁵ G. Mueller,⁵ A. Mukherjee,¹⁵ S. Mukherjee,⁸¹
A. Mullavey,⁶ J. Munch,⁹⁶ D. J. Murphy IV,³⁵ P. G. Murray,³² A. Mytidis,⁵ M. F. Nagy,⁸³ I. Nardecchia,^{66,67}
L. Naticchioni,^{75,25} R. K. Nayak,¹¹⁴ V. Necula,⁵ K. Nedkova,⁹⁵ G. Nelemans,^{11,46} M. Neri,^{40,41} G. Newton,³²
T. T. Nguyen,⁷² A. B. Nielsen,¹⁰ A. Nitz,³¹ F. Nocera,³⁰ D. Nolting,⁶ M. E. N. Normandin,⁸¹ L. K. Nuttall,¹⁶
E. Ochsner,¹⁶ J. O'Dell,¹¹⁵ E. Oelker,¹² G. H. Ogin,¹¹⁶ J. J. Oh,¹¹⁷ S. H. Oh,¹¹⁷ F. Ohme,⁷ M. Okounkova,⁷⁰
P. Oppermann,¹⁰ R. Oram,⁶ B. O'Reilly,⁶ W. E. Ortega,⁸⁵ R. O'Shaughnessy,¹¹⁸ D. J. Ottaway,⁹⁶ R. S. Ottens,⁵
H. Overmier,⁶ B. J. Owen,⁷⁸ C. T. Padilla,²² A. Pai,¹⁰¹ S. A. Pai,⁴² J. R. Palamos,⁵⁴ O. Palashov,¹⁰³ C. Palomba,²⁵
A. Pal-Singh,¹⁰ H. Pan,⁶⁸ Y. Pan,⁵⁷ C. Pankow,¹⁶ F. Pannarale,⁷ B. C. Pant,⁴² F. Paoletti,^{30,19} M. A. Papa,^{26,16}
H. R. Paris,²⁰ A. Pasqualetti,³⁰ R. Passaquieti,^{36,19} D. Passuello,¹⁹ Z. Patrick,²⁰ M. Pedraza,¹ L. Pekowsky,³¹
A. Pele,⁶ S. Penn,¹¹⁹ A. Perreca,³¹ M. Phelps,³² O. Piccinni,^{75,25} M. Pichot,⁴⁷ M. Pickenpack,¹⁰ F. Piergiovanni,^{51,62}
V. Pierro,⁹ G. Pillant,³⁰ L. Pinard,⁵⁹ I. M. Pinto,⁹ M. Pitkin,³² J. H. Poeld,¹⁰ R. Poggiani,^{36,19} A. Post,¹⁰
J. Powell,³² J. Prasad,¹⁴ V. Predoi,⁷ S. S. Premachandra,¹⁰⁷ T. Prestegard,⁷⁹ L. R. Price,¹ M. Prijatelj,³⁰
M. Principe,⁹ S. Privitera,²⁶ R. Prix,¹⁰ G. A. Prodi,^{86,87} L. Prokhorov,⁴³ O. Puncken,^{81,10} M. Punturo,²⁹
P. Puppo,²⁵ M. Pürner,⁷ J. Qin,⁴⁵ V. Quetschke,⁸¹ E. A. Quintero,¹ R. Quitzow-James,⁵⁴ F. J. Raab,³³
D. S. Rabeling,⁷² I. Rácz,⁸³ H. Radkins,³³ P. Raffai,⁴⁸ S. Raja,⁴² M. Rakhmanov,⁸¹ P. Rapagnani,^{75,25}
V. Raymond,²⁶ M. Razzano,^{36,19} V. Re,^{66,67} C. M. Reed,³³ T. Regimbau,⁴⁷ L. Rei,⁴¹ S. Reid,⁴⁴ D. H. Reitze,^{1,5}
F. Ricci,^{75,25} K. Riles,⁶⁵ N. A. Robertson,^{1,32} R. Robie,³² F. Robinet,²³ A. Rocchi,⁶⁷ A. S. Rodger,³² L. Rolland,⁸
J. G. Rollins,¹ V. J. Roma,⁵⁴ R. Romano,^{3,4} G. Romanov,¹¹² J. H. Romie,⁶ D. Rosińska,^{120,37} S. Rowan,³²
A. Rüdiger,¹⁰ P. Ruggi,³⁰ K. Ryan,³³ S. Sachdev,¹ T. Sadecki,³³ L. Sadeghian,¹⁶ M. Saleem,¹⁰¹ F. Salemi,¹⁰
L. Sammut,⁸⁰ E. Sanchez,¹ V. Sandberg,³³ J. R. Sanders,⁶⁵ I. Santiago-Prieto,³² B. Sassolas,⁵⁹ P. R. Saulson,³¹
R. Savage,³³ A. Sawadsky,¹⁷ P. Schale,⁵⁴ R. Schilling,¹⁰ P. Schmidt,¹ R. Schnabel,¹⁰ R. M. S. Schofield,⁵⁴
A. Schönbeck,¹⁰ E. Schreiber,¹⁰ D. Schuette,¹⁰ B. F. Schutz,⁷ J. Scott,³² S. M. Scott,⁷² D. Sellers,⁶ D. Sentenac,³⁰
V. Sequino,^{66,67} A. Sergeev,¹⁰³ G. Serna,²² A. Sevigny,³³ D. A. Shaddock,⁷² P. Shaffery,¹⁰⁸ S. Shah,^{11,46}

M. S. Shahriar,¹⁰² M. Shaltev,¹⁰ Z. Shao,¹ B. Shapiro,²⁰ P. Shawhan,⁵⁷ D. H. Shoemaker,¹² T. L. Sidery,³⁹
 K. Siellez,⁴⁷ X. Siemens,¹⁶ D. Sigg,³³ A. D. Silva,¹³ D. Simakov,¹⁰ A. Singer,¹ L. P. Singer,⁶² R. Singh,²
 A. M. Sintes,⁶⁰ B. J. J. Slagmolen,⁷² J. R. Smith,²² N. D. Smith,¹ R. J. E. Smith,¹ E. J. Son,¹¹⁷ B. Sorazu,³²
 T. Souradeep,¹⁴ A. K. Srivastava,⁹³ A. Staley,³⁵ J. Stebbins,²⁰ M. Steinke,¹⁰ J. Steinlechner,³² S. Steinlechner,³²
 D. Steinmeyer,¹⁰ B. C. Stephens,¹⁶ S. Steplewski,⁵⁰ S. P. Stevenson,³⁹ R. Stone,⁸¹ K. A. Strain,³² N. Straniero,⁵⁹
 N. A. Strauss,⁷³ S. Strigin,⁴³ R. Sturani,¹¹³ A. L. Stuver,⁶ T. Z. Summerscales,¹²¹ L. Sun,⁸⁰ P. J. Sutton,⁷
 B. L. Swinkels,³⁰ M. J. Szczepanczyk,⁵³ M. Tacca,³⁴ D. Talukder,⁵⁴ D. B. Tanner,⁵ M. Tápai,⁹¹ S. P. Tarabrin,¹⁰
 A. Taracchini,²⁶ R. Taylor,¹ T. Theeg,¹⁰ M. P. Thirugnanasambandam,¹ M. Thomas,⁶ P. Thomas,³³
 K. A. Thorne,⁶ K. S. Thorne,⁷⁰ E. Thrane,¹⁰⁷ S. Tiwari,⁷⁴ V. Tiwari,⁵ K. V. Tokmakov,¹⁰⁰ C. Tomlinson,⁸²
 M. Tonelli,^{36,19} C. V. Torres,⁸¹ C. I. Torrie,¹ F. Travasso,^{28,29} G. Traylor,⁶ D. Trifirò,²¹ M. C. Tringali,^{86,87}
 M. Tse,¹² M. Turconi,⁴⁷ D. Ugolini,¹²² C. S. Unnikrishnan,⁹² A. L. Urban,¹⁶ S. A. Usman,³¹ H. Vahlbruch,¹⁰
 G. Vajente,¹ G. Valdes,⁸¹ M. Vallisneri,⁷⁰ N. van Bakel,¹¹ M. van Beuzekom,¹¹ J. F. J. van den Brand,^{56,11}
 C. van den Broeck,¹¹ L. van der Schaaf,¹¹ M. V. van der Sluys,^{11,46} J. van Heijningen,¹¹ A. A. van Veggel,³²
 G. Vansuch,¹²⁶ M. Vardaro,^{123,77} S. Vass,¹ M. Vasúth,⁸³ R. Vaulin,¹² A. Vecchio,³⁹ G. Vedovato,⁷⁷ J. Veitch,³⁹
 P. J. Veitch,⁹⁶ K. Venkateswara,¹²⁴ D. Verkindt,⁸ F. Vetrano,^{51,52} A. Viceré,^{51,52} J.-Y. Vinet,⁴⁷ S. Vitale,¹² T. Vo,³¹
 H. Vocca,^{28,29} C. Vorvick,³³ W. D. Voudsen,³⁹ S. P. Vyatchanin,⁴³ A. R. Wade,⁷² M. Wade,¹⁶ L. E. Wade IV,¹⁶
 M. Walker,² L. Wallace,¹ S. Walsh,¹⁶ G. Wang,⁷⁴ H. Wang,³⁹ M. Wang,³⁹ X. Wang,⁶⁴ R. L. Ward,⁷² J. Warner,³³
 M. Was,⁸ B. Weaver,³³ L.-W. Wei,⁴⁷ M. Weinert,¹⁰ A. J. Weinstein,¹ R. Weiss,¹² T. Welborn,⁶ L. Wen,⁴⁵
 P. Weßels,¹⁰ T. Westphal,¹⁰ K. Wette,¹⁰ J. T. Whelan,^{118,10} D. J. White,⁸² B. F. Whiting,⁵ K. J. Williams,¹¹¹
 L. Williams,⁵ R. D. Williams,¹ A. R. Williamson,⁷ J. L. Willis,¹²⁵ B. Willke,^{17,10} M. H. Wimmer,¹⁰ W. Winkler,¹⁰
 C. C. Wipf,¹ H. Wittel,¹⁰ G. Woan,³² J. Worden,³³ J. Yablon,¹⁰² I. Yakushin,⁶ W. Yam,¹² H. Yamamoto,¹
 C. C. Yancey,⁵⁷ M. Yvert,⁸ A. Zadrożny,¹⁰⁵ L. Zangrando,⁷⁷ M. Zanolin,⁵³ J.-P. Zendri,⁷⁷ Fan Zhang,¹² L. Zhang,¹
 M. Zhang,¹¹² Y. Zhang,¹¹⁸ C. Zhao,⁴⁵ M. Zhou,¹⁰² X. J. Zhu,⁴⁵ M. E. Zucker,¹² S. E. Zuraw,⁹⁵ and J. Zweizig¹

¹*LIGO—California Institute of Technology, Pasadena, CA 91125, USA*

²*Louisiana State University, Baton Rouge, LA 70803, USA*

³*Università di Salerno, Fisciano, I-84084 Salerno, Italy*

⁴*INFN, Sezione di Napoli, Complesso Universitario di Monte S. Angelo, I-80126 Napoli, Italy*

⁵*University of Florida, Gainesville, FL 32611, USA*

⁶*LIGO Livingston Observatory, Livingston, LA 70754, USA*

⁷*Cardiff University, Cardiff CF24 3AA, United Kingdom*

⁸*Laboratoire d'Annecy-le-Vieux de Physique des Particules (LAPP),
Université Savoie Mont Blanc, CNRS/IN2P3, F-74941 Annecy-le-Vieux, France*

⁹*University of Sannio at Benevento, I-82100 Benevento,
Italy and INFN, Sezione di Napoli, I-80100 Napoli, Italy*

¹⁰*Albert-Einstein-Institut, Max-Planck-Institut für Gravitationsphysik, D-30167 Hannover, Germany*

¹¹*Nikhef, Science Park, 1098 XG Amsterdam, The Netherlands*

¹²*LIGO—Massachusetts Institute of Technology, Cambridge, MA 02139, USA*

¹³*Instituto Nacional de Pesquisas Espaciais, 12227-010 São José dos Campos, SP, Brazil*

¹⁴*Inter-University Centre for Astronomy and Astrophysics, Pune 411007, India*

¹⁵*International Centre for Theoretical Sciences, Tata Institute of Fundamental Research, Bangalore 560012, India*

¹⁶*University of Wisconsin-Milwaukee, Milwaukee, WI 53201, USA*

¹⁷*Leibniz Universität Hannover, D-30167 Hannover, Germany*

¹⁸*Università di Siena, I-53100 Siena, Italy*

¹⁹*INFN, Sezione di Pisa, I-56127 Pisa, Italy*

²⁰*Stanford University, Stanford, CA 94305, USA*

²¹*The University of Mississippi, University, MS 38677, USA*

²²*California State University Fullerton, Fullerton, CA 92831, USA*

²³*LAL, Université Paris-Sud, IN2P3/CNRS, F-91898 Orsay, France*

²⁴*University of Southampton, Southampton SO17 1BJ, United Kingdom*

²⁵*INFN, Sezione di Roma, I-00185 Roma, Italy*

²⁶*Albert-Einstein-Institut, Max-Planck-Institut für Gravitationsphysik, D-14476 Golm, Germany*

²⁷*Montana State University, Bozeman, MT 59717, USA*

²⁸*Università di Perugia, I-06123 Perugia, Italy*

²⁹*INFN, Sezione di Perugia, I-06123 Perugia, Italy*

³⁰*European Gravitational Observatory (EGO), I-56021 Cascina, Pisa, Italy*

³¹*Syracuse University, Syracuse, NY 13244, USA*

³²*SUPA, University of Glasgow, Glasgow G12 8QQ, United Kingdom*

³³*LIGO Hanford Observatory, Richland, WA 99352, USA*

- ³⁴ *APC, AstroParticule et Cosmologie, Université Paris Diderot, CNRS/IN2P3, CEA/Irfu, Observatoire de Paris, Sorbonne Paris Cité, F-75205 Paris Cedex 13, France*
- ³⁵ *Columbia University, New York, NY 10027, USA*
- ³⁶ *Università di Pisa, I-56127 Pisa, Italy*
- ³⁷ *CAMK-PAN, 00-716 Warsaw, Poland*
- ³⁸ *Astronomical Observatory Warsaw University, 00-478 Warsaw, Poland*
- ³⁹ *University of Birmingham, Birmingham B15 2TT, United Kingdom*
- ⁴⁰ *Università degli Studi di Genova, I-16146 Genova, Italy*
- ⁴¹ *INFN, Sezione di Genova, I-16146 Genova, Italy*
- ⁴² *RRCAT, Indore MP 452013, India*
- ⁴³ *Faculty of Physics, Lomonosov Moscow State University, Moscow 119991, Russia*
- ⁴⁴ *SUPA, University of the West of Scotland, Paisley PA1 2BE, United Kingdom*
- ⁴⁵ *University of Western Australia, Crawley, Western Australia 6009, Australia*
- ⁴⁶ *Department of Astrophysics/IMAPP, Radboud University Nijmegen, P.O. Box 9010, 6500 GL Nijmegen, The Netherlands*
- ⁴⁷ *ARTEMIS, Université Nice-Sophia-Antipolis, CNRS and Observatoire de la Côte d'Azur, F-06304 Nice, France*
- ⁴⁸ *MTA Eötvös University, "Lendület" Astrophysics Research Group, Budapest 1117, Hungary*
- ⁴⁹ *Institut de Physique de Rennes, CNRS, Université de Rennes 1, F-35042 Rennes, France*
- ⁵⁰ *Washington State University, Pullman, WA 99164, USA*
- ⁵¹ *Università degli Studi di Urbino 'Carlo Bo', I-61029 Urbino, Italy*
- ⁵² *INFN, Sezione di Firenze, I-50019 Sesto Fiorentino, Firenze, Italy*
- ⁵³ *Embry-Riddle Aeronautical University, Prescott, AZ 86301, USA*
- ⁵⁴ *University of Oregon, Eugene, OR 97403, USA*
- ⁵⁵ *Laboratoire Kastler Brossel, UPMC-Sorbonne Universités, CNRS, ENS-PSL Research University, Collège de France, F-75005 Paris, France*
- ⁵⁶ *VU University Amsterdam, 1081 HV Amsterdam, The Netherlands*
- ⁵⁷ *University of Maryland, College Park, MD 20742, USA*
- ⁵⁸ *Center for Relativistic Astrophysics and School of Physics, Georgia Institute of Technology, Atlanta, GA 30332, USA*
- ⁵⁹ *Laboratoire des Matériaux Avancés (LMA), IN2P3/CNRS, Université de Lyon, F-69622 Villeurbanne, Lyon, France*
- ⁶⁰ *Universitat de les Illes Balears—IEEC, E-07122 Palma de Mallorca, Spain*
- ⁶¹ *Università di Napoli 'Federico II', Complesso Universitario di Monte S. Angelo, I-80126 Napoli, Italy*
- ⁶² *NASA/Goddard Space Flight Center, Greenbelt, MD 20771, USA*
- ⁶³ *Canadian Institute for Theoretical Astrophysics, University of Toronto, Toronto, Ontario M5S 3H8, Canada*
- ⁶⁴ *Tsinghua University, Beijing 100084, China*
- ⁶⁵ *University of Michigan, Ann Arbor, MI 48109, USA*
- ⁶⁶ *Università di Roma Tor Vergata, I-00133 Roma, Italy*
- ⁶⁷ *INFN, Sezione di Roma Tor Vergata, I-00133 Roma, Italy*
- ⁶⁸ *National Tsing Hua University, Hsinchu Taiwan 300*
- ⁶⁹ *Charles Sturt University, Wagga Wagga, New South Wales 2678, Australia*
- ⁷⁰ *Caltech—CaRT, Pasadena, CA 91125, USA*
- ⁷¹ *Pusan National University, Busan 609-735, Korea*
- ⁷² *Australian National University, Canberra, Australian Capital Territory 0200, Australia*
- ⁷³ *Carleton College, Northfield, MN 55057, USA*
- ⁷⁴ *INFN, Gran Sasso Science Institute, I-67100 L'Aquila, Italy*
- ⁷⁵ *Università di Roma 'La Sapienza', I-00185 Roma, Italy*
- ⁷⁶ *University of Brussels, Brussels 1050, Belgium*
- ⁷⁷ *INFN, Sezione di Padova, I-35131 Padova, Italy*
- ⁷⁸ *Texas Tech University, Lubbock, TX 79409, USA*
- ⁷⁹ *University of Minnesota, Minneapolis, MN 55455, USA*
- ⁸⁰ *The University of Melbourne, Parkville, Victoria 3010, Australia*
- ⁸¹ *The University of Texas at Brownsville, Brownsville, TX 78520, USA*
- ⁸² *The University of Sheffield, Sheffield S10 2TN, United Kingdom*
- ⁸³ *Wigner RCP, RMKI, H-1121 Budapest, Konkoly Thege Miklós út 29-33, Hungary*
- ⁸⁴ *Montclair State University, Montclair, NJ 07043, USA*
- ⁸⁵ *Argentinian Gravitational Wave Group, Cordoba Cordoba 5000, Argentina*
- ⁸⁶ *Università di Trento, Dipartimento di Fisica, I-38123 Povo, Trento, Italy*
- ⁸⁷ *INFN, Trento Institute for Fundamental Physics and Applications, I-38123 Povo, Trento, Italy*
- ⁸⁸ *The Pennsylvania State University, University Park, PA 16802, USA*
- ⁸⁹ *University of Chicago, Chicago, IL 60637, USA*
- ⁹⁰ *University of Cambridge, Cambridge CB2 1TN, United Kingdom*

- ⁹¹ *University of Szeged, Dóm tér 9, Szeged 6720, Hungary*
⁹² *Tata Institute for Fundamental Research, Mumbai 400005, India*
⁹³ *Institute for Plasma Research, Bhat, Gandhinagar 382428, India*
⁹⁴ *American University, Washington, D.C. 20016, USA*
⁹⁵ *University of Massachusetts-Amherst, Amherst, MA 01003, USA*
⁹⁶ *University of Adelaide, Adelaide, South Australia 5005, Australia*
⁹⁷ *West Virginia University, Morgantown, WV 26506, USA*
⁹⁸ *Korea Institute of Science and Technology Information, Daejeon 305-806, Korea*
⁹⁹ *University of Białystok, 15-424 Białystok, Poland*
¹⁰⁰ *SUPA, University of Strathclyde, Glasgow G1 1XQ, United Kingdom*
¹⁰¹ *IISER-TVM, CET Campus, Trivandrum Kerala 695016, India*
¹⁰² *Northwestern University, Evanston, IL 60208, USA*
¹⁰³ *Institute of Applied Physics, Nizhny Novgorod, 603950, Russia*
¹⁰⁴ *Hanyang University, Seoul 133-791, Korea*
¹⁰⁵ *NCBJ, 05-400 Świerk-Otwock, Poland*
¹⁰⁶ *IM-PAN, 00-956 Warsaw, Poland*
¹⁰⁷ *Monash University, Victoria 3800, Australia*
¹⁰⁸ *Seoul National University, Seoul 151-742, Korea*
¹⁰⁹ *ESPCI, CNRS, F-75005 Paris, France*
¹¹⁰ *Università di Camerino, Dipartimento di Fisica, I-62032 Camerino, Italy*
¹¹¹ *Southern University and A&M College, Baton Rouge, LA 70813, USA*
¹¹² *College of William and Mary, Williamsburg, VA 23187, USA*
¹¹³ *Instituto de Física Teórica, University Estadual Paulista/ICTP South American Institute for Fundamental Research, São Paulo SP 01140-070, Brazil*
¹¹⁴ *IISER-Kolkata, Mohanpur, West Bengal 741252, India*
¹¹⁵ *Rutherford Appleton Laboratory, HSIC, Chilton, Didcot, Oxon OX11 0QX, United Kingdom*
¹¹⁶ *Whitman College, 280 Boyer Ave, Walla Walla, WA 9936, USA*
¹¹⁷ *National Institute for Mathematical Sciences, Daejeon 305-390, Korea*
¹¹⁸ *Rochester Institute of Technology, Rochester, NY 14623, USA*
¹¹⁹ *Hobart and William Smith Colleges, Geneva, NY 14456, USA*
¹²⁰ *Institute of Astronomy, 65-265 Zielona Góra, Poland*
¹²¹ *Andrews University, Berrien Springs, MI 49104, USA*
¹²² *Trinity University, San Antonio, TX 78212, USA*
¹²³ *Università di Padova, Dipartimento di Fisica e Astronomia, I-35131 Padova, Italy*
¹²⁴ *University of Washington, Seattle, WA 98195, USA*
¹²⁵ *Abilene Christian University, Abilene, TX 79699, USA*
¹²⁶ *Emory University, Atlanta, GA 30322, USA*

We report results of a wideband search for periodic gravitational waves from isolated neutron stars within the Orion spur towards both the inner and outer regions of our Galaxy. As gravitational waves interact very weakly with matter, the search is unimpeded by dust and concentrations of stars. One search disk (A) is 6.87° in diameter and centered on $20^{\text{h}}10^{\text{m}}54.71^{\text{s}} + 33^\circ33'25.29''$, and the other (B) is 7.45° in diameter and centered on $8^{\text{h}}35^{\text{m}}20.61^{\text{s}} - 46^\circ49'25.151''$. We explored the frequency range of 50-1500 Hz and frequency derivative from 0 to -5×10^{-9} Hz/s. A multi-stage, *loosely coherent* search program allowed probing more deeply than before in these two regions, while increasing coherence length with every stage.

Rigorous followup parameters have winnowed initial coincidence set to only 70 candidates, to be examined manually. None of those 70 candidates proved to be consistent with an isolated gravitational wave emitter, and 95% confidence level upper limits were placed on continuous-wave strain amplitudes. Near 169 Hz we achieve our lowest 95% CL upper limit on worst-case linearly polarized strain amplitude h_0 of 6.3×10^{-25} , while at the high end of our frequency range we achieve a worst-case upper limit of 3.4×10^{-24} for all polarizations and sky locations.

I. INTRODUCTION

In this paper we report the results of a deep search along the Orion spur for continuous, nearly monochromatic gravitational waves in data from LIGO's sixth science (S6) run. The search covered frequencies from 50 Hz through 1500 Hz and frequency derivatives from 0 Hz/s through -5×10^{-9} Hz/s.

Our solar system is located in the Orion spur — a

spoke-like concentration of stars connecting the Sagittarius and Perseus arms of our galaxy. Since known pulsars tend to be found in concentrations of stars such as galactic arms and globular clusters [1, 2], the Orion spur offers a potential target. This search explores a portion of the Orion spur towards the inner regions of our Galaxy as well as a nearly opposite direction covering the Vela nebula.

A number of searches have been carried out previ-

ously on LIGO data [3–11], including coherent searches for gravitational waves from known radio and X-ray pulsars. An Einstein@Home search running on the BOINC infrastructure [12] has performed blind all-sky searches on data from LIGO’s S4 and S5 science runs [13–15].

The results in this paper were produced with the PowerFlux search code. It was first described in [3] together with two other semi-coherent search pipelines (Hough, Stackslide). The sensitivities of all three methods were compared, with PowerFlux showing better results in frequency bands lacking severe spectral artifacts. A subsequent article [5] based on the data from the S5 run featured improved upper limits and a systematic follow-up detection search based on the *Loosely coherent* algorithm [16].

In this paper we establish the most sensitive wide-band upper limits to date in the frequency band 50-1500 Hz. Near 169 Hz our strain sensitivity to a neutron star with the most unfavorable sky location and orientation (“worst case”) yields a 95% confidence level upper limit in intrinsic strain amplitude of 6.3×10^{-25} , while at the high end of our frequency range we achieve a worst-case upper limit of 3.4×10^{-24} .

Starting from 94,000 outliers surviving the first stage of the pipeline, only 70 survived the fourth and final stage of the automated search program and were then examined manually for instrumental contamination. Of the 70 outliers found, several do not have an easily identifiable instrumental cause.

Deeper follow-ups of the outliers do not lead to increased statistical significance, as would be expected for a GW-emitting isolated neutron star. Accurate estimation of the probability for a statistical fluctuation to lead to the loudest of these outliers, using simulation of the search on independent data sets, is computationally infeasible, but a rough (conservative) estimate (described in section V) is $O(10\%)$. Given this modest improbability and given the inconsistency of deep follow-up results with the isolated signal model, we conclude that statistical fluctuations are a likely explanation for these outliers.

As the deeper follow-up searches assumed a tight coherence length, this leaves open a narrow window for the outliers to be caused by neutron star with an additional frequency modulation such as would be observed if it were in long-period orbit. The enlargement of parameter-space needed to cover this possibility makes it impractical to test this hypothesis with S6 data.

II. LIGO INTERFEROMETERS AND S6 SCIENCE RUN

The LIGO gravitational wave network consists of two observatories, one in Hanford, Washington and the other in Livingston, Louisiana, separated by a 3000-km baseline. During the S6 run each site housed one suspended interferometer with 4-km long arms.

Although the sixth science run spanned more than one

year period of data acquisition, the analysis in this paper used data only from GPS 951534120 (2010 Mar 02 03:01:45 UTC) through GPS 971619922 (2010 Oct 20 14:25:07 UTC), selected for good strain sensitivity and noise stationarity. Since interferometers sporadically fall out of operation (“lose lock”) due to environmental or instrumental disturbances or for scheduled maintenance periods, the data set is not contiguous. For the time span used in the search the Hanford interferometer H1 had a duty factor of 53%, while the Livingston interferometer L1 had a duty factor of 51%. The strain sensitivity in search band was not uniform, exhibiting a $\sim 50\%$ daily variation from anthropogenic activity as well as gradual improvement toward the end of the run [19, 21].

A thorough description of instruments and data can be found in [20].

III. SEARCH REGION

All-sky searches for continuous gravitational waves in data produced by modern interferometers are computationally limited, with the established upper limits an order of magnitude away from what is theoretically possible given impractically large computational resources. This limitation arises from the rapid increase in computational cost with coherence time of the search, because of both the necessarily finer gridding of the sky and the need to search over higher-order derivatives of the signal frequency. Hence there is a tradeoff between searching the largest sky area with reduced sensitivity of all-sky search, and pushing for sensitivity in a smaller region.

The loosely coherent search program was initially developed for follow-up of outliers from an all-sky semi-coherent search [5]. For this search we have chosen to isolate two small regions and take advantage of the enhanced sensitivity of the loosely coherent search. Besides the gain from increasing coherence length we also benefit from search regions (listed in Table I) with strong Doppler-modulated frequency evolution and greater rejection of instrumental artifacts.

Known radio pulsars tend to cluster along the spiral arms, in globular clusters, and in other star-forming regions. To increase the chances of discovering a continuous wave gravitational source we selected regions where one can expect a clustering of neutron star sources in line-of-sight cones determined by the search area and sensitivity reach of the detector.

The positions of known pulsars from the ATNF catalog ([22, 23], retrieved 2015 Jan 29) and the expected reach of semicoherent searches are illustrated in Figure 1 on the galactic background [24]. Only pulsars with galactic latitude less than 0.06 rad are shown in the figure. We observe loose association with galactic arms, which is skewed by observational bias. In particular, the area searched by Parkes survey marked as a blue sector contains many more pulsars than elsewhere on the map.

The expected reach of the all-sky search in S6 data,

Search region	RA rad	DEC rad	Radius rad	RA hours	DEC deg	Radius deg
A	5.283600	0.585700	0.060	20 ^h 10 ^m 54.715 ^s	33°33′29.297″	3.438
B	2.248610	-0.788476	0.065	8 ^h 35 ^m 20.607 ^s	-46°49′25.151″	3.724

TABLE I. Area of sky covered by this search.

assuming a neutron star ellipticity of 10^{-6} , is illustrated by the pink circle. A computationally feasible spotlight search can reach twice as far, but the globular clusters and galactic center remain out of its reach in the S6 data set.

A closer alternative is to look in the local neighbourhood of the Sun along the Orion spur — a grouping of stars that connects the Perseus and Sagittarius arms of our galaxy. For this search we have chosen two regions (Table I), exploring two nearly opposite directions along the Orion spur.

Region A was chosen to point near Cygnus X, with region B pointing toward the Vela nebula I. A recent study of OB stars and their ramifications for local supernova rates support these two directions as potentially promising, along with several other star-forming regions [2]. The choice of sky area to search for region B is more ambiguous because of larger extent of Orion spur — the figure 1 shows two grouping of stars towards the Vela Molecular Ridge and Perseus transit directions. We have chosen the direction towards Vela as it coincides with star forming region with several known neutron stars. In order to better cover Vela nebula the region B search radius is slightly larger than that of region A.

IV. SEARCH ALGORITHM

The results presented in this paper were obtained with the loosely coherent search, implemented as part of the PowerFlux program. We have used the follow-up procedure developed for the all-sky S6 search, but where the first loosely coherent stage is applied directly to the entire A and B regions. A detailed description of the loosely coherent code can be found in [5, 16].

Mathematically, we transform the input data to the Solar System barycentric reference frame, correct for putative signal evolution given by frequency, spindown and polarization parameters, and then apply a low-pass filter which bandwidth determines the coherence length of the search. The total power in the computed time series is then compared to power obtained for nearby frequency bins in a 0.25 Hz interval.

A signal-to-noise ratio and an upper limit are derived for each frequency bin using a universal statistic method [25] that establishes 95% CL upper limit for an arbitrary underlying noise distribution. If the noise is Gaussian distributed the upper limits are close to optimal values that would be produced with assumption of Gaussianity.

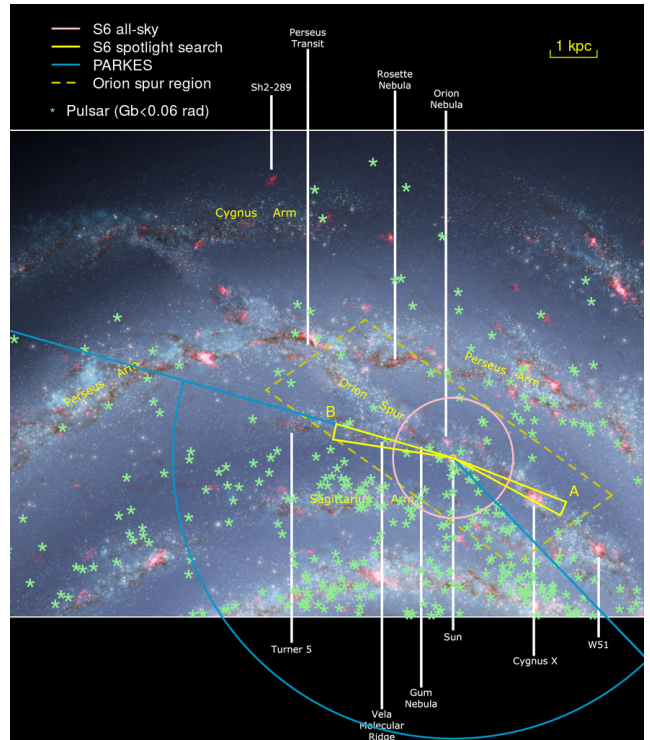


FIG. 1. Distribution of known pulsars in the Milky Way galaxy. The Orion spur region (marked by dashed rectangle) connects Perseus and Sagittarius galactic arms and includes regions marked A and B. The ranges shown for gravitational wave searches correspond to 1500 Hz frequency and an ellipticity of 10^{-6} . The arc shown for the PARKES survey [1] shows search area, not the range. The green stars show locations of pulsars from the ATNF database (retrieved on January 29, 2015, [22]) with galactic latitude Gb below 0.06 radians. The background image is due to R. Hurt [24] (color online)

For non-Gaussian noise the upper limits are conservatively correct.

Maxima of the SNR and upper limits over marginalized search parameters are presented in the plots 2, 3 and 4.

The search results described in this paper assume a classical model of a spinning neutron star with a fixed, non-axisymmetric mass quadrupole that produces circularly polarized gravitational waves along the rotation axis and linearly polarized radiation in the directions perpendicular to the rotation axis. The assumed signal model

is thus

$$h(t) = h_0 \left(F_+(t, \alpha, \delta, \psi) \frac{1+\cos^2(\iota)}{2} \cos(\Phi(t)) + F_\times(t, \alpha, \delta, \psi) \cos(\iota) \sin(\Phi(t)) \right), \quad (1)$$

where F_+ and F_\times characterize the detector responses to signals with “+” and “ \times ” quadrupolar polarizations, the sky location is described by right ascension α and declination δ , ι describes the inclination of the source rotation axis to the line of sight, and the phase evolution of the signal is given by the formula

$$\Phi(t) = 2\pi(f_{\text{source}}(t - t_0) + f^{(1)}(t - t_0)^2/2) + \phi, \quad (2)$$

with f_{source} being the source frequency and $f^{(1)}$ denoting the first frequency derivative (for which we also use the abbreviation *spindown*). ϕ denotes the initial phase with respect to reference time t_0 . t is time in the solar system barycenter frame. When expressed as a function of local time of ground-based detectors it includes the sky-position-dependent Doppler shift. We use ψ to denote the polarization angle of the projected source rotation axis in the sky plane.

As a first step, individual SFTs (short Fourier transforms) with high noise levels or large spikes in the underlying data are removed from the analysis. For a typical well-behaved frequency band, we can exclude 8% of the SFTs while losing only 4% of the accumulated statistical weight. For a band with large detector artifacts (such as instrumental lines arising from resonant vibration of mirror suspension wires), however, we can end up removing most, if not all, SFTs. As such bands are not expected to have any sensitivity of physical interest they were excluded from the upper limit analysis (Table II).

Category	Description
60 hz line	59.75-60.25 Hz
Violin modes	343.25-343.75 Hz, 347 Hz
Second harmonic of violin modes	687.00-687.50 Hz
Third harmonic of violin modes	1031.00-1031.25 Hz

TABLE II. Frequency regions excluded from upper limit analysis. These are separated into power line artifacts and harmonics of “violin modes” (resonant vibrations of the wires which suspend the many mirrors of the interferometer).

The detection pipeline used in this search was developed for an S6 all-sky analysis and is an extension of the pipeline described in [5]. It consists of several stages employing loosely coherent [16] search algorithm with progressively stricter coherence requirements. The parameters of the pipeline are described in Table III.

Unlike in the all-sky analysis the first stage is used to establish upper limits. In effect, instead of investigating all-sky outliers we have simply pointed the follow-up pipeline along the direction of Orion spur. This allowed us to increase the sensitivity by a factor of 2. The rest of the pipeline is unmodified.

The frequency refinement parameter is specified relative to the 1/1800 Hz frequency bin width used in SFTs that serve as input to the analysis. Thus at the last stage of follow-up our frequency resolution is $(1800 \text{ s} \cdot 32)^{-1} = 17 \mu\text{Hz}$. However, because of the degeneracy between frequency, sky position and spindown, the accuracy is not as good and the frequency can deviate by up to 50 μHz in 95% of injections. This degeneracy is mostly due to Doppler shifts from Earth orbital motion and is thus common to both interferometers.

The phase coherence parameter δ is described in detail in [16]. It represents the amount of allowed phase variation over a 1800 s interval. We are thus sensitive both to the expected sources with ideal frequency evolution (equation 2) and unexpected sources with a small amount of frequency modulation.

The sky refinement parameter is relative to the sky resolution sufficient for the plain semi-coherent PowerFlux mode and was necessary because the improved frequency resolution made the search more sensitive to Doppler shift.

Stages one and two used the same parameters, with the only difference being that data acquired at nearby times by different interferometers were combined without regard to phase in stage 1, but we took phase into account in stage 2. In the ideal situation, when both detectors are operational at the same time and at the same sensitivity, one would expect an increase in SNR by $\sqrt{2}$ by including phase information. In practice, the duty cycle did not overlap perfectly and, most importantly, it was quite common for one interferometer to be more sensitive than another. Thus, to keep an outlier, we only required that SNR did not decrease when transitioning to stage 2.

Subsequent stages used longer coherence times, with correspondingly finer sky and frequency resolutions.

The analysis data set was partitioned in time into 7 parts of equal duration numbered 0 through 6. As an intermediate product we have obtained upper limits and outliers of each contiguous sequence of parts. For example, a segment [1,5] would consist of the middle 5/7 of the entire data set. This allowed us to identify outliers that exhibited enhanced SNR on a subset of data and thus were more likely to be induced by instrumental artifacts (Tables V and VI).

V. GAUSSIAN FALSE ALARM EVENT RATE

The computation of the false alarm rate for the outliers passing all stages of the pipeline is complicated by the fact that most outliers are caused by instrumental artifacts for which we do not know the underlying probability distribution. In principle, one could repeat the analysis many times using non-physical frequency shifts (which would exclude picking up a real signal by accident) in order to obtain estimates of false alarm rate, but this approach incurs prohibitive computational cost. Even assuming a perfect Gaussian background, it is dif-

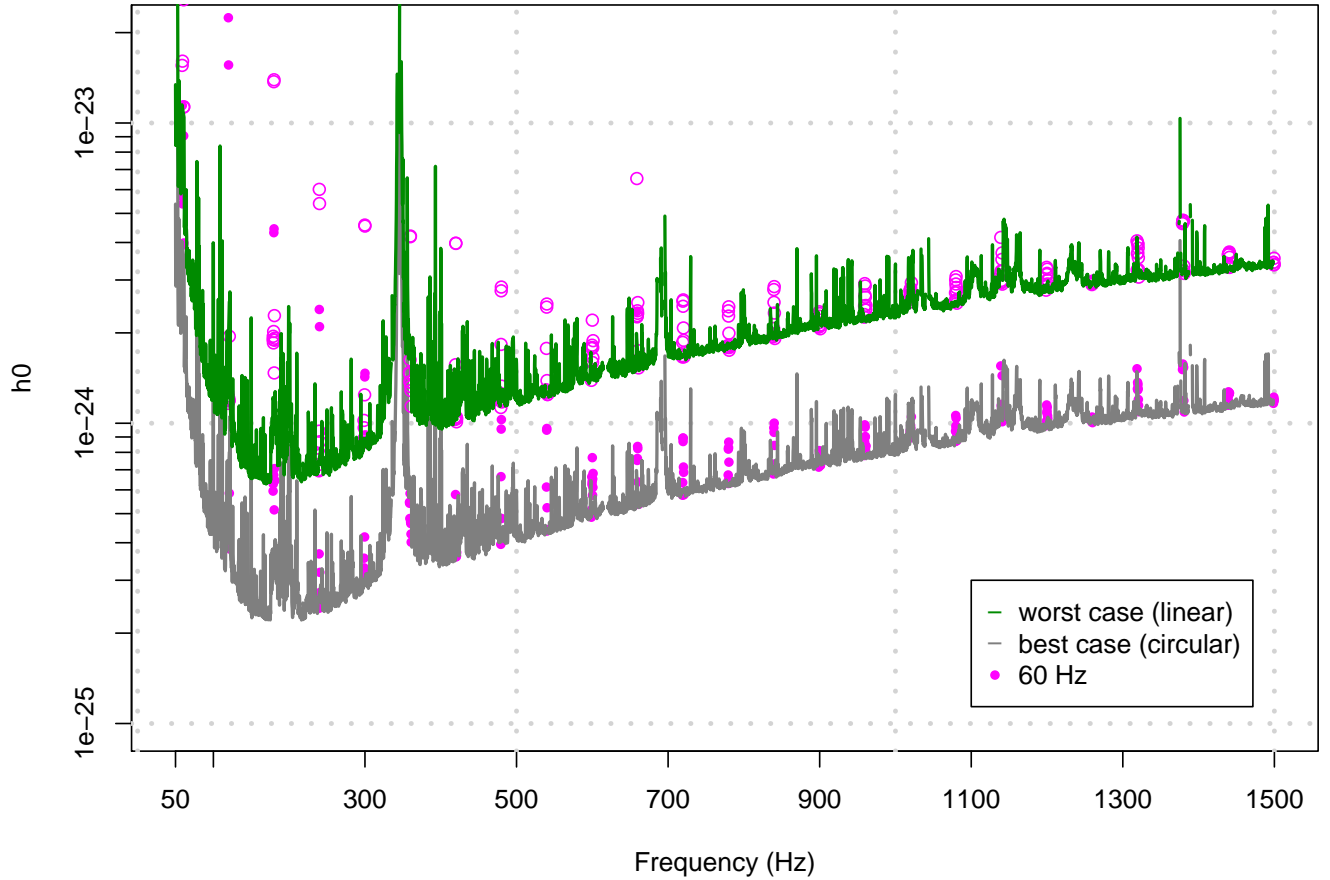


FIG. 2. S6 95% CL upper limits on signal strain amplitude. The upper (green) curve shows worst case upper limits in analyzed 0.25 Hz bands (see Table II for list of excluded bands). The lower (grey) curve shows upper limits assuming circularly polarized source. The values of solid points and circles (marking power line harmonics for circularly and linear polarized sources) are not considered reliable. They are shown to indicate contaminated bands. (color online)

Stage	Instrument sum	Phase coherence rad	Spindown step Hz/s	Sky refinement	Frequency refinement	SNR increase %
1	incoherent	$\pi/2$	1.0×10^{-10}	1/4	1/8	NA
2	coherent	$\pi/2$	5.0×10^{-11}	1/4	1/8	0
3	coherent	$\pi/4$	2.5×10^{-11}	1/8	1/16	12
4	coherent	$\pi/8$	5.0×10^{-12}	1/16	1/32	12

TABLE III. Analysis pipeline parameters. All stages used the loosely coherent algorithm for demodulation. The sky and frequency refinement parameters are relative to values used in the semicoherent PowerFlux search.

difficult to model the pipeline in every detail to obtain an accurate estimate of the false alarm rate, given the gaps in interferometer operations and non-stationary noise.

Instead, we compute a figure of merit that overestimates the actual Gaussian false alarm event rate. We

simplify the problem by assuming that the entire analysis was carried out with the resolution of the very last stage of follow-up and we are merely triggering on the SNR value of the last stage. This is extremely conservative as we ignore the consistency requirements that allow

the outlier to proceed from one stage of the pipeline to the next, actual false alarm rate could be lower.

The SNR of each outlier is computed relative to the loosely coherent power sum for 501 frequency bins spaced at 1/1800 Hz intervals (including the outlier) but with all the other signal parameters held constant. The spacing assures that any sub-bin leakage does not affect the statistics of the power sum.

As the power sums are weighted, the statistics should follow a weighted χ^2 distribution, the exact shape of which is difficult to characterize analytically because the weights depend on sky position, gaps in acquired data, background noise in the SFTs and the polarization parameters of the outlier.

To simplify computation we assume that we are dealing with a simple χ^2 distribution with the number of degrees of freedom given by the timebase divided by the coherence length and multiplied by a conservative duty factor reflecting interferometer uptime and the worst-case weights from linearly-polarized signals.

Thus to find the number of degrees of freedom we will use the formula

$$N \approx \frac{\text{timebase} \cdot \delta \cdot \text{duty factor}}{1800 \text{ s} \cdot 2\pi} \quad (3)$$

with the duty factor taken to be 0.125 and δ giving the phase coherence parameter of the loosely coherent search. The duty factor was chosen to allow for only 50% interferometer uptime and only one quarter of the data receiving high weights from our weighting scheme, which weights the contribution of data inversely as the square of the estimated noise [17, 18].

The number of search templates that would be needed if the last stage of follow-up were used on the entire search region is conservatively (over)estimated as

$$K = 5.8 \times 10^7 \frac{f_1^3 - f_0^3}{1400.25^3 - 1400^3} \quad (4)$$

where f_0 and f_1 (in Hz) describe the frequency band of interest. For any particular 0.25 Hz search band the number of templates scales quadratically in frequency due to linearly growing influence of Doppler shifts. Thus the integrated frequency dependence is cubic. The scaling factor 5.8×10^7 was obtained by counting the number of templates for a particular PowerFlux instance that searched from 1400 Hz to 1400.25 Hz. For the entire analysis $f_0 = 50$ Hz and $f_1 = 1500$ Hz, which yields $K = 1.3 \times 10^{11}$ templates, without accounting for template overlap.

Thus we define the outlier figure of merit describing Gaussian false alarm event rate as

$$\text{GFA} = K \cdot P_{\chi^2} \left(N + \text{SNR} \cdot \sqrt{2N}; N \right) \quad (5)$$

where N defines the number of degrees of freedom as given by equation 3, $P_{\chi^2}(x; N)$ gives the probability for

a χ^2 distribution with N degrees of freedom to exceed x , and K describes the estimated number of templates.

We point out that the GFA is overly conservative when applied to frequency bands with Gaussian noise, but is only loosely applicable to bands with detector artifacts, which can affect both the estimate of the degrees of freedom of the underlying distribution and the assumption of uncorrelated underlying noise.

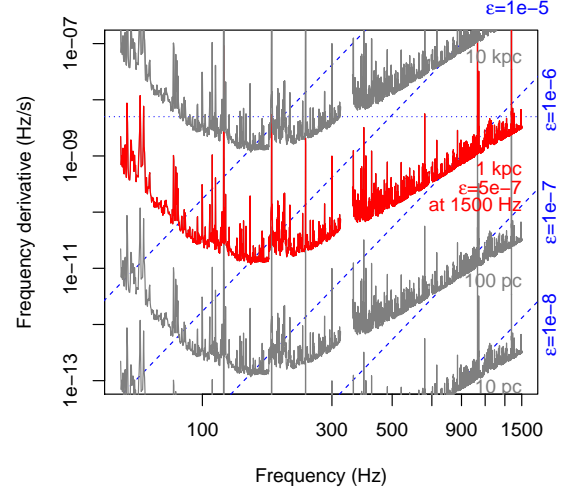


FIG. 3. Range of the PowerFlux search for neutron stars spinning down solely due to gravitational waves. This is a superposition of two contour plots. The grey and red solid lines are contours of the maximum distance at which a neutron star in optimum orientation could be detected as a function of gravitational-wave frequency f and its derivative \dot{f} . The dashed lines are contours of the corresponding ellipticity $\epsilon(f, \dot{f})$. The fine dotted line marks the maximum spin-down searched. Together these quantities tell us the maximum range of the search in terms of various populations (see text for details). In particular, at 1500 Hz we are sensitive to stars with ellipticity of 5×10^{-7} up to 1 kpc away. (color online)

VI. RESULTS

Stage	Region A	Region B
1	43884	51027
2	7921	9152
3	510	566
4	37	33

TABLE IV. Outlier counts found at each stage of follow up.

PowerFlux produces 95% confidence level upper limits

for individual templates, where each template represents a particular value of frequency, spindown, sky location and polarization. The results are maximized over several parameters, and a correction factor is applied to account for possible mismatches between a true signal and sampled parameters. Figure 2 shows the resulting upper limits maximized over the analyzed spindown range, over the search regions and, for the upper curve, over all sampled polarizations. The lower curve shows the upper limit for circular polarized signals alone.

The numerical data for this plot can be obtained separately [26].

The regions near harmonics of the 60 Hz power mains frequency are shown as circles.

Figure 3 provides an easy way to judge the astrophysical range of the search. We have computed the implied spindown solely due to gravitational emission at various distances, as well as corresponding ellipticity curves, assuming a circularly polarized signal. This follows formulas in paper [3]. For example, at the highest frequency sampled, assuming ellipticity of 5×10^{-7} (which is well under the maximum limit in [27, 28]) we can see as far as 1000 parsecs.

In each search band, including regions with detector artifacts, the follow-up pipeline was applied to outliers satisfying the initial coincidence criteria. The outlier statistics are given in Table IV. The outliers that passed all stages of the automated pipeline are listed in Table V for the A direction and Table VI for the B direction. Each of these outliers was inspected manually and tested against further criteria to determine whether it was convincingly due to a source in the targeted astrophysical population.

Tables V and VI list outlier index (an identifier used during follow-up), signal-to-noise ratio, decimal logarithm of Gaussian false alarm as computed by formula 5, the contiguous segment of data where the outlier had the highest SNR (see below), frequency, spindown, right ascension and declination, as well as a summary of manual follow-up conclusions.

The segment column describes the persistence of the outlier throughout the analysis. The data to be analyzed was divided into seven equal-duration segments labeled 0 through 6. For a continuous signal, the maximum SNR is achieved by integrating all segments: this is indicated by the notation [0,6]. For a transient artifact [29], one can achieve higher SNR by analyzing only those segments when it was on. This case is indicated by noting the continuous set of segments that gives the largest SNR: e.g. [1,5] if a higher SNR is achieved by dropping the first and last segment. Note, however, that an astrophysical signal such as a long-period binary may also appear more strongly in some segments than others, and thus could have a segment notation other than [0,6]. The same will be true of a strong signal outside of the search area on the sky, whose Doppler shifts happen to align with the target area's over some segment of time. This occurs, for instance, with outliers A1 and A3, which were generated by a strong simulated signal outside of the search area.

For a low SNR continuous signal it is also possible for the background noise to randomly align in such a way that the SNR over [0,6] segment is slightly lower than on a smaller subset. Our simulations show that 98.5% of injections achieve maximum SNR over one of [0,6], [0,5] or [1,6] segments.

Outliers marked as non-Gaussian were found to lie in bands whose statistics deviated from Gaussian noise, according to the following criterion: the excess kurtosis of 501 bins around the outlier was smaller than -1.05 . The probability of Gaussian sample having this excess kurtosis is smaller than 10^{-6} .

If manual inspection of an outlier indicated that it overlaps with a strong spectral disturbance in one of the detectors, this is noted in the tables. Disturbances might be either narrow lines, or steep slopes or edges characteristic of wandering lines or the wings of nearby spectral features. When such contamination is manifestly obvious under visual inspection, it is likely that the outlier was due to that artifact rather than an astrophysical signal. Outliers with identified contamination are marked with comments in Tables V and VI.

Two of the outliers were induced by very loud simulated hardware injections. The true parameters of these signals are listed in Table VII.

VII. MANUAL OUTLIER FOLLOWUP

To determine whether or not any of the outliers in Tables V and VI indicated a credible gravitational wave detection, each outlier was subjected to manual inspection, after which several criteria were used to eliminate those not likely due to the target astrophysical population. First, we discarded any candidate with a segment other than [0,6], [0,5], or [1,6]: as noted, this would eliminate less than 1.5% of true signals from our population. Next, we disregard those signals marked as "non-Gaussian". This criterion has a more substantial false dismissal probability: roughly 20% of the search band was so marked. Nonetheless, we would be unable to claim with any confidence that a candidate from such a band was *not* simply a non-Gaussian instrumental outlier. Finally, we disregard outliers in bands with visually obvious spectral disturbances: this has a similar false dismissal rate, but has substantial overlap with the non-Gaussian bands.

This winnowing resulted in three surviving candidates: A14, A27, and A29. Of these, A14 is the most interesting (Figure 4), with a $\log_{10}(\text{GFA})$ of -0.9 . This suggests that, conservatively, roughly 10% of searches of this type would produce an outlier as loud as A14 due to Gaussian noise alone. While not enough to make a confident claim of detection, this was certainly enough to motivate further follow-up.

All three candidates were followed up with NO-MAD [15, 33], a hierarchical pipeline used in previous continuous-wave searches [15]. This adaptive pipeline

Idx	SNR	$\log_{10}(\text{GFA})$	Segment	Frequency Hz	Spindown nHz/s	RA_{J2000} degrees	$\text{DEC}_{\text{J2000}}$ degrees	Description
1	194.1	-188.8	[0, 0]	108.83151	-3.090	323.755	37.114	Induced by loud hardware injection 3
3	32.1	-27.3	[0, 1]	192.55507	-0.585	306.480	34.197	Induced by loud hardware injection 8
4	31.3	-36.8	[2, 5]	69.73917	-2.885	313.580	16.478	Line in L1, Non Gaussian
6	14.7	-7.3	[2, 5]	988.82017	0.215	307.682	33.630	Line in H1, Non Gaussian
7	11.4	-2.9	[2, 6]	648.74939	-5.000	299.622	33.315	Line in H1
8	10.8	-1.2	[2, 5]	1143.32783	-0.995	300.553	32.632	Strong disturbance in H1
9	10.2	1.4	[0, 1]	481.96422	-0.105	301.872	34.275	Line in L1, disturbed background in H1 and L1
10	10.2	0.5	[2, 4]	99.14832	-1.100	318.949	27.088	Disturbed background in L1
11	9.8	0.3	[1, 4]	897.63729	-2.215	303.190	35.780	Non Gaussian
12	9.8	1.0	[2, 4]	956.74358	-4.115	302.033	34.395	Disturbed background in H1, Non Gaussian
13	9.8	-0.7	[1, 6]	1138.50993	0.090	299.389	34.748	Disturbed background in H1+L1, Non Gaussian
14	9.7	-0.9	[0, 6]	1404.89226	-1.205	303.637	36.819	
15	9.6	-0.8	[0, 6]	799.42915	-0.840	300.724	31.062	Line in H1, Non Gaussian
16	9.5	0.1	[1, 5]	1368.77913	-3.560	304.484	30.949	Lines in H1
17	9.4	2.4	[1, 2]	1308.96651	-1.670	304.436	30.232	Non Gaussian
18	9.4	0.8	[2, 5]	1386.45871	-0.510	304.398	34.228	Line in H1 at 1386.5 Hz, Non Gaussian
21	9.2	2.6	[5, 6]	1170.98217	-4.395	304.353	34.829	Non Gaussian
22	9.0	4.1	[2, 2]	1191.26642	-0.455	300.720	31.494	
23	8.9	2.1	[0, 2]	829.72137	-2.900	305.831	33.090	
24	8.9	0.4	[0, 6]	1321.56703	-1.820	304.707	32.001	Non Gaussian
25	8.9	2.9	[4, 5]	1058.43325	-3.600	300.356	31.068	
26	8.9	1.6	[1, 4]	1302.65337	-2.250	299.854	34.786	
27	8.8	0.9	[0, 5]	1474.94224	-2.050	303.295	32.273	
28	8.8	0.6	[0, 6]	990.76130	-2.705	299.638	33.235	Disturbed background in H1
29	8.7	1.1	[1, 6]	1429.67892	-2.010	303.739	32.845	
30	8.6	0.9	[0, 6]	1325.50969	-4.325	300.291	34.313	Disturbed background in L1, Non Gaussian
31	8.5	3.4	[5, 6]	1177.15326	-0.040	307.054	32.374	
32	8.4	1.5	[1, 6]	1330.69434	-3.285	300.625	34.037	Disturbed background in H1, Non Gaussian
33	8.4	1.5	[0, 5]	1456.26611	0.195	302.336	33.628	L1 SNR is inconsistent with background level
34	8.3	2.0	[2, 6]	995.14313	-1.400	302.428	31.768	Disturbed background in L1
35	8.1	1.8	[0, 6]	1286.17215	-1.185	305.624	35.126	Line in H1, Non Gaussian
36	8.0	2.8	[2, 5]	1386.02201	0.050	304.242	36.465	Line in H1 at 1385.9 Hz, Non Gaussian
37	7.8	4.2	[1, 2]	1359.72387	-1.745	298.903	32.885	Instrumental contamination in L1

TABLE V. Outliers that passed the full detection pipeline from region A. Only the highest-SNR outlier is shown for each 0.1 Hz frequency region. Outliers marked with “line” had strong narrowband disturbance identified near outlier location. Outliers marked as “non Gaussian” were identified as having non Gaussian statistic in their power sums, often due to very steeply sloping spectrum.

searched a span of 255 days of S6 data in 5 successive stages of refinement: with coherent segment lengths of 2.5 days, 5 days, 7.5 days, 10 days, 12.5 days, and 255 days (fully coherent). The recovered power from each candidate remained roughly constant at each stage, and consistent with noise, rather than increasing with coherence length. This strongly indicates that these outliers do not follow the presumed signal model over timescales of several days.

As a consistency check we have also studied the outliers with long coherence codes based on \mathcal{F} -statistic [8, 30, 31, 33] as well as codes with shorter coherence lengths [32]. The search [34] with coherence time of 27 days established upper limits at the outlier locations ruling out any significant signals.

VIII. CONCLUSIONS

We have performed the first deep search along the Orion spur for continuous gravitational waves in the range 50-1500 Hz, achieving a factor of 2 improvement over results from all-sky searches. Exploring a large spin-down range, we placed upper limits on both expected and unexpected sources. At the highest frequencies we are sensitive to neutron stars with an equatorial ellipticity as small as 5×10^{-7} and as far away as 1000 pc for favorable spin orientations.

A detection pipeline based on a loosely coherent algorithm was applied to outliers from our search. Three outliers (A14, A27, and A29 on Table V) were found with continuous presence and no obvious instrumental contamination. However, deeper follow-up did not reveal a source consistent with the original signal model. This, combined with the only modest improbability of the loud-

Idx	SNR	$\log_{10}(\text{GFA})$	Segment	Frequency Hz	Spindown nHz/s	RA_{J2000} degrees	$\text{DEC}_{\text{J2000}}$ degrees	Description
1	41.3	-55.9	[1, 4]	243.27113	-3.675	134.486	-35.443	Line in H1
3	19.8	-20.9	[0, 6]	69.74870	-4.130	111.634	-36.471	Line in L1, Non Gaussian
4	15.3	-6.8	[1, 3]	268.96658	-5.065	135.288	-46.431	Line in H1
5	11.7	-2.5	[2, 5]	170.84304	-2.725	124.589	-48.321	H1 SNR is larger than coherent sum
6	11.3	0.2	[2, 3]	108.07698	-0.115	122.585	-48.207	Disturbed background in H1
7	10.9	-2.0	[1, 5]	158.39427	-3.550	122.974	-49.793	Line in H1
8	10.8	2.5	[0, 0]	1111.39559	-0.345	131.270	-44.537	
9	10.8	2.5	[3, 3]	956.81519	-0.905	129.372	-44.282	Disturbed background in H1
10	10.6	2.7	[3, 3]	950.80278	-1.900	128.821	-45.115	Disturbed background in H1
11	10.5	2.8	[0, 0]	611.12967	0.255	130.848	-49.230	Non Gaussian
12	10.0	-0.6	[2, 6]	1076.04377	-3.250	133.282	-47.130	Line in L1 at 1076 Hz, Non Gaussian
13	9.9	3.3	[3, 3]	1118.06896	-2.645	128.952	-47.992	Disturbed background in L1
14	9.6	0.0	[2, 6]	1498.30429	-2.000	131.393	-48.022	Disturbed background in L1
15	9.6	-0.7	[0, 6]	613.26132	-3.950	125.353	-42.144	Non Gaussian
16	9.3	0.4	[2, 6]	1498.73031	-0.195	125.668	-42.539	Non Gaussian
17	9.3	0.0	[0, 5]	933.33823	0.100	127.556	-48.783	Non Gaussian
18	9.1	1.3	[0, 3]	1313.24312	-5.000	127.562	-47.859	Disturbed background in H1
19	8.9	1.6	[0, 3]	1458.79267	-2.425	125.394	-43.661	
20	8.9	0.8	[1, 6]	1249.43835	-1.550	128.846	-46.928	Disturbed background in H1+L1, Non Gaussian
21	8.7	1.1	[1, 6]	880.40175	-2.865	130.890	-47.472	Disturbed background in H1, Non Gaussian
22	8.6	2.5	[2, 4]	1254.11705	-1.295	128.862	-41.615	Line in L1, Non Gaussian
23	8.6	1.3	[1, 6]	1333.27906	-1.650	128.265	-47.879	Non Gaussian
24	8.6	3.3	[1, 2]	1497.14217	-2.210	129.202	-46.366	Line in H1, Non Gaussian
25	8.6	3.3	[2, 3]	1333.83095	-4.445	124.636	-46.522	Non Gaussian
26	8.4	1.8	[0, 4]	1336.24255	-0.005	126.374	-42.633	Non Gaussian
27	8.3	4.7	[1, 1]	1370.69201	-3.375	130.199	-41.568	
28	8.3	2.1	[1, 5]	1316.98962	-1.025	130.853	-47.324	Non Gaussian
29	8.2	4.9	[2, 2]	795.42245	-3.855	131.083	-47.536	
30	8.2	1.6	[0, 6]	1458.53648	-3.800	131.684	-43.218	Line in H1
31	8.1	2.0	[0, 5]	1119.11347	-3.975	125.384	-43.551	Disturbed background in L1
32	7.9	3.0	[2, 5]	1331.56844	-4.210	128.647	-46.135	Disturbed background in H1
33	7.6	3.8	[3, 5]	1334.83602	-4.700	129.188	-41.911	

TABLE VI. Outliers that passed the full detection pipeline from region B. Only the highest-SNR outlier is shown for each 0.1 Hz frequency region. Outliers marked with “line” had strong narrowband disturbance identified near outlier location. Outliers marked as “non Gaussian” were identified as having non Gaussian statistic in their power sums, often due to very steeply sloping spectrum.

Name	Frequency Hz	Spindown Hz/s	RA_{J2000} degrees	$\text{DEC}_{\text{J2000}}$ degrees
ip3	108.85716	-1.46×10^{-17}	178.37	-33.44
ip8	193.48479	-8.65×10^{-09}	351.39	-33.42

TABLE VII. Parameters of hardware-injected simulated signals detected by PowerFlux (epoch GPS 846885755).

est outlier occurring in Gaussian noise, leads us to conclude that statistical fluctuations are the likely explanation for these outliers.

IX. ACKNOWLEDGMENTS

The authors gratefully acknowledge the support of the United States National Science Foundation for the construction and operation of the LIGO Laboratory, the Science and Technology Facilities Council of the United Kingdom, the Max-Planck-Society, and the State

of Niedersachsen/Germany for support of the construction and operation of the GEO600 detector, and the Italian Istituto Nazionale di Fisica Nucleare and the French Centre National de la Recherche Scientifique for the construction and operation of the Virgo detector. The authors also gratefully acknowledge the support of the research by these agencies and by the Australian Research Council, the International Science Linkages program of the Commonwealth of Australia, the Council of Scientific and Industrial Research of India, the Istituto Nazionale di Fisica Nucleare of Italy, the Spanish Ministerio de Educación y Ciencia, the Conselleria d’Economia Hisenda

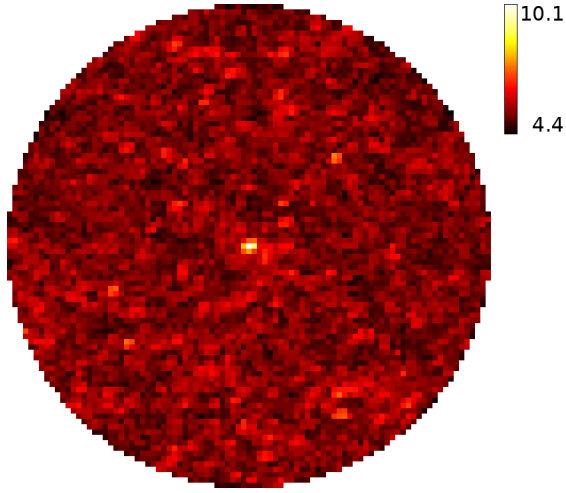


FIG. 4. SNR skymap for outlier A 14. The disk (0.025 rad radius) is centered on the location of the signal. Each pixel (0.555 mrad) on the skymap shows the SNR maximized over a 5×5 template sub-grid and all polarizations. The high frequency of the signal (1404 Hz) allows good localization (color online)

i Innovació of the Govern de les Illes Balears, the Foundation for Fundamental Research on Matter supported by the Netherlands Organisation for Scientific Research, the Polish Ministry of Science and Higher Education, the FOCUS Programme of Foundation for Polish Science, the Royal Society, the Scottish Funding Council, the Scottish Universities Physics Alliance, The National Aeronautics and Space Administration, the Carnegie Trust, the Leverhulme Trust, the David and Lucile Packard Foundation, the Research Corporation, and the Alfred P. Sloan Foundation.

This document has been assigned LIGO Laboratory document number LIGO-P1500034-v23.

-
- [1] D. R. Lorimer, A. J. Faulkner, A. G. Lyne, R. N. Manchester, M. Kramer, M. A. McLaughlin, G. Hobbs, A. Posenti, I. H. Stairs, F. Camilo, M. Burgay, N. D'Amico, A. Corongiu, F. Crawford, MNRAS, **372**, 777 (2006)
 - [2] J. G. Schmidt, M. M. Hohle, R. Neuhauser, Astron. Nachr. / AN **999**, No. 88 (2006)
 - [3] B. Abbott *et al.* (LIGO Scientific Collaboration), Phys. Rev. D **77**, 022001 (2008).
 - [4] B. P. Abbott *et al.* (LIGO Scientific Collaboration), Phys. Rev. Lett. **102**, 111102 (2009).
 - [5] J. Abadie *et al.* (The LIGO and Virgo Scientific Collaboration), Phys. Rev. D **85**, 022001 (2012)
 - [6] B. Abbott *et al.* (LIGO Scientific Collaboration), M. Kramer, and A. G. Lyne, Phys. Rev. Lett. **94**, 181103 (2005).
 - [7] B. Abbott *et al.* (LIGO Scientific Collaboration), M. Kramer, and A. G. Lyne, Phys. Rev. D **76**, 042001 (2007).
 - [8] B. Abbott *et al.* (LIGO Scientific Collaboration), Phys. Rev. D **76**, 082001 (2007).
 - [9] B. Abbott *et al.* (LIGO Scientific Collaboration), Astrophys. J. Lett. **683**, 45 (2008).
 - [10] B. P. Abbott *et al.* (LIGO Scientific Collaboration and Virgo Collaboration), Astrophys. J. **713**, 671 (2010).
 - [11] J. Abadie *et al.* (LIGO Scientific Collaboration), Astrophys. J. **722**, 1504 (2010).
 - [12] The Einstein@Home project is built upon the BOINC (Berkeley Open Infrastructure for Network Computing) architecture described at <http://boinc.berkeley.edu/>.
 - [13] B. Abbott *et al.* (LIGO Scientific Collaboration), Phys. Rev. D **79**, 022001 (2009).
 - [14] B. P. Abbott *et al.* (LIGO Scientific Collaboration), Phys. Rev. D **80**, 042003 (2009).
 - [15] B. P. Abbott *et al.* (LIGO Scientific Collaboration), Phys. Rev. D **87**, 042001 (2013).
 - [16] V. Dergachev, Class. Quantum Grav. **27**, 205017 (2010).
 - [17] V. Dergachev, LIGO technical document LIGO-T050186 (2005), available in <https://dcc.ligo.org/>
 - [18] V. Dergachev, LIGO technical document LIGO-T1000272 (2010), available in <https://dcc.ligo.org/>
 - [19] J. Abadie *et al.* (LIGO Scientific Collaboration and Virgo Collaboration), arXiv:1203.2674 [gr-qc], <http://arxiv.org/abs/1203.2674>
 - [20] J. Aasi *et al.* (LIGO Scientific Collaboration and Virgo Collaboration), arXiv:1410.7764 [gr-qc], <http://arxiv.org/abs/1410.7764>
 - [21] B. Abbott *et al.* (LIGO Scientific Collaboration), Rep. Prog. Phys. **72**, 076901 (2009).
 - [22] R.N. Manchester, G.B. Hobbs, A. Teoh, M. Hobbs, Astron. J. **129**, 1993-2006 (2005)
 - [23] ATNF catalog is available at <http://www.atnf.csiro.au/research/pulsar/psrcat>
 - [24] NASA/JPL-Caltech/R. Hurt <http://www.spitzer.caltech.edu/images/1925-ssc2008-10b-A-Roadmap-to-the-Milky-Way-Annotated->
 - [25] V. Dergachev, Phys. Rev. D **87**, 062001 (2013).
 - [26] See EPAPS Document No. [number will be inserted by publisher] for numerical values of upper limits.
 - [27] C. J. Horowitz and K. Kadau, Phys. Rev. Lett. **102**, 191102 (2009).
 - [28] N. K. Johnson-McDaniel and B. J. Owen, Phys. Rev. D **88**, 044004 (2013)
 - [29] R. Prix, S. Giampanis, and C. Messenger, Phys. Rev. D **84**, 023007 (2011)
 - [30] P. Jaranowski, A. Królak, and B. F. Schutz, Phys. Rev. D **58**, 063001 (1998).
 - [31] C. Cutler, B. F. Schutz, Phys. Rev. D **72**, 063006 (2005)
 - [32] J. Abadie *et al.* (LIGO Scientific Collaboration and Virgo

- Collaboration), Physical Review Letters, **107**, 271102 (2011)
- [33] M. Shaltev, R. Prix, Phys. Rev. D **87**, 084057 (2013).
- [34] J. Aasi *et al.* (LIGO Scientific Collaboration and the Virgo Collaboration), arXiv:1412.5942 [astro-ph.HE], <http://arxiv.org/abs/1412.5942>